CMS Physics Analysis Summary

Contact: cms-pag-conveners-exotica@cern.ch 2016/03/17

Search for new physics in high mass diphoton events in 3.3 fb^{-1} of proton-proton collisions at $\sqrt{s} = 13$ TeV and combined interpretation of searches at 8 TeV and 13 TeV

The CMS Collaboration

Abstract

We report on a search for new physics using high mass diphoton events. The search employs 3.3 fb^{-1} of pp collision data collected by the CMS experiment in 2015 at a center-of-mass energy of 13 TeV. It is aimed at spin-0 and spin-2 resonances of mass between 500 and 4500 GeV and relative width up to 5.6×10^{-2}. The results of the search are combined with those obtained by the CMS collaboration in similar searches at $\sqrt{s} = 8$ TeV.

1 Introduction

The resonant production of high mass diphoton pairs is a generic prediction of several extensions of the standard model (SM) of particle physics. From very general assumptions [1, 2], the spin of a resonance decaying to two photons can be restricted to be either 0 or an integer greater or equal to 2. The production of heavy scalar resonances decaying to two photons is predicted by SM extensions with non-minimal Higgs sectors, while the production of spin-2 resonances is predicted by models postulating the existence of additional space-like dimensions.

Theories that introduce additional space-like dimensions provide an approach to solve the so-called hierarchy problem, which has its origin in the large difference between the scale of the electroweak and of the gravitational interactions. The existence of additional dimensions has the effect of "diluting" gravity and thus allows lowering of the scale of the gravitational interaction and avoidance of the hierarchy problem.

Two families of models, introduced by Arkani-Hamed, Dimopoulos and Dvali (ADD) [3], and by Randall and Sundrum (RS) [4] have been developed. In the first, the additional dimensions are assumed to be flat and compact. By allowing the gravitational field to propagate in the extra dimensions, the large difference between the Planck and electroweak scales can be explained. In the RS model, the presence of two brane-worlds is postulated and the SM fields are allowed to propagate in only one of the two. The further assumption of a warped space-time metric allows the difference between the electroweak and Planck scales to be accounted for. From the phenomenological point of view, both families predict that the excitations of the gravitational field lead to "towers" of spin-2 resonances, commonly denoted as gravitons, separated by a characteristic mass scale [5–9].

In the case of the ADD model, the mass separation is so small that individual resonances cannot be resolved from each other. In the diphoton final state this would lead to the observation of a broad excess in the invariant mass spectrum over the SM continuum. In the case of the RS model, the mass separation is large enough to allow the independent observation of each resonance.

The simplest extension of the SM Higgs sector consists in the addition of a second doublet of scalar fields to the theory. Models of this kind, known as two-Higgs-doublet models (2HDM) [10] feature the presence of a total of five scalar or pseudo-scalar resonances in the spectrum of the theory. Identifying one of the scalars as the 125 GeV Higgs boson discovered by the CMS and ATLAS collaborations [11, 12], and assuming that its couplings correspond to those of the SM Higgs boson, forces the 2HDM in the so-called alignment limit [13] where some of the additional resonances can decay to a diphoton pair at a non-negligible rate.

Recently, the ATLAS [14] and CMS [15] collaborations reported the results on searches for diphoton resonances at $\sqrt{s} = 13$ TeV, in the mass ranges $200\,\text{GeV} - 2\,\text{TeV}$ and $500\,\text{GeV} - 4.5\,\text{TeV}$ respectively. In the former case, the search is interpreted in terms of spin-0 resonances produced through the same mechanisms leading to the SM Higgs boson production. In the latter, the analysis is interpreted in terms of production of RS graviton resonances. Both analyses reported the observation of modest deviations from the background-only expectations, compatible with the resonant production of two photons. In case of the ATLAS analysis, the largest deviation from the background-only hypotheses is observed for a resonance with a mass of 750 GeV and it has a local statistical significance between 3.6 and 3.9 standard deviations, depending on the width hypothesis. In the case of the CMS analysis, the largest excess is reported for a narrow resonance of mass of around 760 GeV and it has a local statistical significance of about 2.6 standard deviations.

Searches for RS graviton production were performed at lower centre of mass energies by the CMS and ATLAS collaborations in proton-proton collisions and by the CDF and D0 collaborations in proton-antiproton collisions, using final states containing pairs of photons, leptons, jets or vector bosons [16–26]. Searches for scalar particles decaying to two photons were also performed by the CMS and ATLAS collaborations at lower centre of mass energies [16, 27]. The deviations at $\sqrt{s} = 13$ TeV that were reported in Ref. [14, 15] are compatible with previous results, under the hypothesis that they are due to the decay of a new resonance produced mostly through gluon-gluon fusion.

The results reported in this note are based on $3.3\,\text{fb}^{-1}$ of pp collisions collected by the CMS experiment in 2015 at $\sqrt{s} = 13$ TeV. They extend and supersede those previously reported by the CMS collaboration [15]. The use of a new detector calibration and the inclusion in the analysis of additional data, recorded while the CMS magnet was not operated, improved the sensitivity of the analysis by more than 20% with respect to the previous results.

The results obtained on the $\sqrt{s} = 13$ TeV dataset are combined statistically with those obtained by the CMS collaboration in similar searches carried out at $\sqrt{s} = 8$ TeV [16, 17].

2 The CMS detector

The central feature of the CMS apparatus is a superconducting solenoid of 6 m internal diameter, providing a magnetic field of 3.8 T. Within the superconducting solenoid volume are a silicon pixel and strip tracker, a lead tungstate crystal electromagnetic calorimeter (ECAL), and a brass and scintillator hadron calorimeter (HCAL), each composed of a barrel and two endcap sections. Forward calorimeters (HF) extend the pseudorapidity [28] coverage provided by the barrel and endcap detectors. Muons are measured in gas-ionization detectors embedded in the steel flux-return yoke outside the solenoid.

In the barrel section of the ECAL, an energy resolution of about 1% is achieved for unconverted or late-converting photons in the tens of GeV energy range. The remaining barrel photons have an energy resolution of about 1.3% up to a pseudorapidity of $|\eta| = 1$, rising to about 2.5% at $|\eta| = 1.4$. In the endcaps, the resolution of unconverted or late-converting photons is about 2.5%, while the remaining endcap photons have a resolution between 3 and 4% [29]. The dynamic range of the ECAL readout electronics allows to measure the energy deposited in single crystals in the barrel (endcaps) region between a few tens of MeV and roughly 2(3) TeV.

The particle-flow event algorithm [30, 31] reconstructs and identifies each individual particle with an optimised combination of information from the various elements of the CMS detector. The energy of photons is directly obtained from the ECAL measurement, correcting for radiative losses and containment effects. The energy of electrons is determined from a combination of the electron momentum at the primary interaction vertex as determined by the tracker, the energy of the corresponding ECAL cluster, and the energy sum of all bremsstrahlung photons spatially compatible with originating from the electron track. The energy of muons is obtained from the curvature of the corresponding track. The energy of charged hadrons is determined from a combination of their momentum measured in the tracker and the matching ECAL and HCAL energy deposits, corrected for zero-suppression effects and for the response function of the calorimeters to hadronic showers. Finally, the energy of neutral hadrons is obtained from the corresponding corrected ECAL and HCAL energy.

The first level (L1) of the CMS trigger system, composed of custom hardware processors, uses information from the calorimeters and muon detectors to select the most interesting events

in a fixed time interval of less than 4 μs. The high level trigger (HLT) processor farm further decreases the event rate from around 100 kHz to around 300 Hz, before data storage.

A more detailed description of the CMS detector, together with a definition of the coordinate system used and the relevant kinematic variables, can be found in Ref. [28].

3 Data and simulated samples

The data considered in this analysis correspond to an integrated luminosity of 3.3 fb^{-1} collected by the CMS experiment in 2015. The dataset fulfills standard quality criteria for all components of the CMS detector, except in a fraction of the dataset for the HF calorimeter. Part of the dataset, corresponding to 2.7 fb^{-1}, was recorded while the CMS magnet was operated at 3.8T, while a second part of the dataset, amounting to 0.6 fb^{-1}, was recorded while the CMS magnet was off.

Samples with simulated production of spin-0 and spin-2 resonances decaying to two photons were generated with PYTHIA 8.2 [32] using the NNPDF2.3 [33] parton distribution functions (PDFs). Several samples were generated, spanning signal hypotheses in the range where 500 GeV $< m <$ 4.5 TeV and $0.14 \times 10^{-4} < \Gamma/m < 5.6 \times 10^{-2}$. The ranges of masses and widths were chosen to match those tested in the analysis reported in Ref. [15]. The set of tested widths is obtained assuming the values of 0.01, 0.1 and 0.2 for $\tilde{\kappa}$, the reduced graviton coupling in the RS model [9].

The processes giving rise to background in the search for the resonant diphoton production are the irreducible background from the direct production of two photons as well as the reducible components due to $\gamma +$ jets and multi-jet final states, where jet fragments are misidentified as photons. Simulated background samples were used for the optimisation of the analysis and to study the systematic uncertainties related to the background estimation. The background from prompt diphoton processes was generated using SHERPA 2.1 [34]. The MADGRAPH5 2.2 [35] generator, interfaced with PYTHIA, was used to model the production of $\gamma +$ jets. In both cases additional hard emissions, up to three additional partons in the final state, were generated at leading order (LO) in perturbative QCD and the NNPDF3.0 [36] PDFs were used. Multi-jet final states were modelled using PYTHIA with NNPDF2.3 PDFs. The PYTHIA tune CUETP8M1 [37] was used.

A detailed simulation of the CMS detector response to the events in the signal and background samples was performed using the GEANT4 package [38]. The average number of interactions per bunch crossing in the dataset is 11.4, with an RMS of 2.1. Simulated events include the effect of multiple proton-proton interactions (pileup) taking place each bunch crossing and were weighted to reproduce the distribution of the number of interactions per bunch crossing in data.

4 Event selection and reconstruction

Events with at least two reconstructed photon candidates are selected and a search is made for a localised excess of events in the diphoton mass spectrum consistent with the resonant production of diphoton pairs.

For the B = 3.8 T (B = 0 T) dataset, the trigger selection requires at least two photon candidates of transverse momentum above 60(40) GeV. For these events, the ratio between the energy deposited in the hadron calorimeter towers behind each the photon candidate and the photon

energy ("H/E ratio") is required to be less than 0.15. The trigger selection is fully efficient for resonances of mass above 500 GeV.

Photon candidates are reconstructed from energy deposits in the ECAL. Energy deposits compatible with the expected shower shape of electrons and photons are clustered together. The clustering algorithm does not make any hypothesis as to whether the particle originating from the interaction point is a photon or an electron. Thus the same algorithm used for photon reconstruction can be applied to $Z \to e^+e^-$ events and these events can be used to measure the efficiency of the photon selection criteria and of the photon energy scale and resolution.

In order to obtain the best energy resolution, the ECAL signals are calibrated and corrected for several detector effects. The variation of the crystal transparency during the run is corrected with a dedicated monitoring system and the single-channel response equalised using collision events [29]. With respect to the results reported in Ref. [15], the data were re-reconstructed using single-channel response calibration coefficients derived using the full dataset recorded in 2015.

The containment of the shower in the clustered crystals, the shower losses for photons that convert in the material upstream of the calorimeter, and the effects of pileup, are corrected for using a multivariate regression technique [29]. Photons of very high energy can deposit in a single crystals higher energy than can be measured by the ECAL digitization electronics. In this case, the estimated photon energy can be significantly lower than the true one and its variance very large. A dedicated multivariate regression was developed to correct for the effect. Using simulated events it is found that after the application of the corrections, the energy scale of photons where saturation of the ECAL electronics has occurred deviates from unity by less than 2% and the energy resolution is better than 3%. However, saturation occurred for none of the photon candidates selected in this analysis.

As mentioned earlier, the mean number of pp interactions per bunch crossing is 11.4 in the analysed dataset. In the longitudinal direction, z, the interaction vertices, built from the reconstructed tracks, have a distribution with an RMS spread of about 5 cm. The diphoton mass resolution has contributions from the resolution of the measurement of the photon energies and the measurement of the angle between the two photons. If the vertex from which the photons originate is known to within about 10 mm, then the experimental resolution on the angle between them makes a negligible contribution to the mass resolution. Associating the diphoton with one of the vertices reconstructed from the charged particle tracks in the event satisfies this requirement since the position of these vertices is measured with far greater precision.

In the $B = 3.8\,T$ dataset, the interaction vertex is selected using the algorithm described in Refs. [39, 40], which relies on the knowledge of the tracks momenta. Due to the lack of such information, a simpler algorithm is used for the $B = 0\,T$ dataset and the interaction vertex with the largest track multiplicity is selected. For resonances of masses above 500 GeV, the fraction of events in which the interaction vertex is correctly assigned is approximately 90(60)% for the $B = 3.8\,T$ ($B = 0\,T$) dataset.

For the $B = 3.8\,T$ dataset, the modelling of the vertex-finding algorithm is verified using dimuon events, where the vertexes are re-reconstructed following removal of the muon tracks, so that the event mimics a diphoton event, and $\gamma +$ jets events. For the $B = 0\,T$ dataset, the performance of the algorithm is verified using di-electron events where the vertexes are re-reconstructed after the removal of the electrons tracks. Figure 1 shows, for di-electron events in the $B = 0\,T$ sample, the comparison of the vertex finding efficiency between data and simulated events, as a function of the transverse momentum of the pair. Here the vertex finding efficiency

is defined as the probability that the z coordinate of the chosen vertex is within 10 mm of the true one.

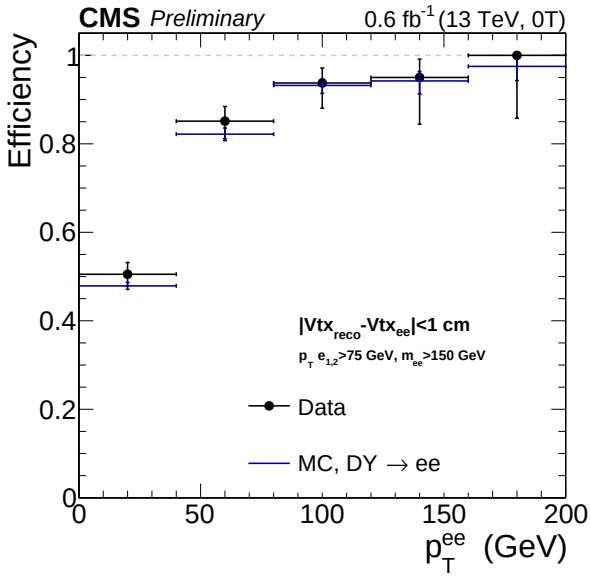

Figure 1: Efficiency to find the correct vertex within 1 cm for dielectron pairs with an invariant mass above 150 GeV in the B = 0 T dataset as a function of the dielectron transverse momentum. Data and simulated events are shown.

Photon candidates are organised in pairs, which are required to satisfy the following kinematic criteria:

- The p_T of both candidates is required to be above 75 GeV.
- The absolute value of the pseudorapidity of both candidates, computed with respect to centre of the CMS detector and denoted $|\eta_{SC}|$ in the following, is required to be below 2.5 and not between 1.44 and 1.57.
- At least one of the photon candidates is required to have $|\eta_{SC}|$ below 1.44 (i.e. events with both photon candidates in the ECAL endcaps regions are rejected).
- The invariant mass of the pair, $m_{\gamma\gamma}$, is required to be above 230 GeV. For events where one of the photon candidates is in an endcap, $m_{\gamma\gamma} > 320$ GeV is required.

Photon candidates are further required to satisfy different sets identification criteria, depending on whether the data was recorded at B = 3.8 T or at B = 0 T. For the B = 3.8 T dataset the following criteria are to be satisfied:

- The transverse size of the electromagnetic cluster in the η direction is required to be compatible with that expected from prompt photons.
- The H/E ratio is required to be less than 0.05.
- The sum of the transverse momenta (I_{Ch}) of particle-flow charged hadron candidates contained in a cone of radius 0.3 in η, ϕ space centred on the photon candidates is required to be below 5 GeV. Charged particle-flow candidates compatible with conversion tracks associated with the photon candidates are excluded from the sum.
- The sum of the transverse energy of additional photon candidates contained in regions of radius 0.3 in η, ϕ, corrected for pileup effects, is required to be below 2.5 GeV.
- Photon candidates associated with electron tracks incompatible with conversion

tracks are rejected.

For the B = 0 T dataset the set of identification criteria is instead the following:

- The transverse size of the electromagnetic cluster, in both the η and ϕ directions, is required to be compatible with that expected from prompt photons.
- The number of reconstructed tracks contained in a cone of radius 0.3 in η, ϕ space centred on the photon candidates is required to be at most 3. Tracks compatible with conversion tracks associated with the photon candidates are excluded from the sum.
- The sum of the transverse energy of additional photon candidates contained in regions of radius 0.3 in η, ϕ is required to be below 3.6(3) GeV for photon candidates in the barrel (endcap) region.
- Photon candidates associated with electron tracks incompatible with conversion tracks are rejected.

In the B = 3.8 T dataset the efficiency of the identification criteria for prompt isolated photon candidates, in the kinematic range considered by the analysis, is above 90(85)% in the barrel (endcaps). In the B = 0 T dataset, the identification efficiency is above about 85(70)% for prompt isolated photon candidates in the barrel (endcaps). The identification and trigger efficiencies are measured using events containing a pair of electrons, or pair of muon or electron candidates in association with a photon candidate. The efficiencies measured in data are found to be compatible with the predicted ones within uncertainties.

The fraction of events where more than one diphoton pair satisfies the selection criteria is roughly 1%. In these cases, only the pair with the largest scalar sum of photon momenta is retained. Diphoton pairs are split into two categories: the first, denoted "EBEB" in the following, contains pairs where both candidates are reconstructed in the ECAL barrel, while the second, denoted "EBEE", contains pairs where one of the candidates is reconstructed in an ECAL endcap. Each category is further split to separate events recorded at B = 3.8 T and at B = 0 T. The fraction of signal events selected in each of the analysis categories is shown in Fig. 2 for different signal hypotheses.

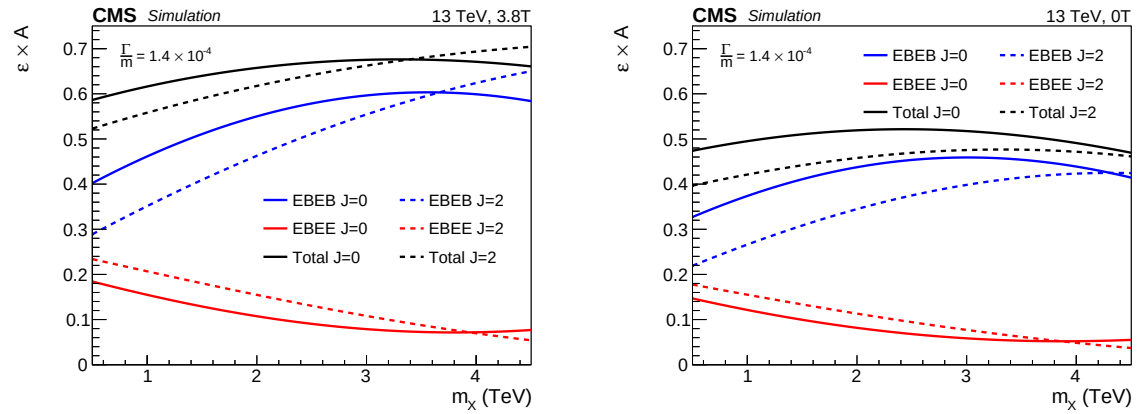

Figure 2: Fraction of events selected by the analysis categories for 500 GeV $< m <$ 4.5 TeV and $\Gamma/m = 1.4 \times 10^{-4}$. Curves for both spin-0 and RS graviton resonances are shown, on the left for the B = 3.8 T sample and on the right for the B = 0 T one.

The selection criteria were determined using simulated signal and background samples and fixed prior to inspecting the diphoton invariant mass distribution in the search region, which is defined as $m_{\gamma\gamma} > 500$ GeV. The level of agreement between data and simulation was assessed

before inspecting the diphoton invariant mass distribution in the search region. The evaluation was performed by checking other distributions in the search region, as well as all distributions for events outside of the search region. The event selection efficiencies were measured in data and compared with expectations and the ratio of the total number of expected and observed events in the search region were checked as part of the procedure. In the case of the $B = 3.8\,T$ dataset, the background composition was also measured and compared with predictions. None of these assessments led to a change in the selection criteria that were determined using simulated events.

5 Determination of the photon energy scale and resolution

As described above, the energy of the photon candidates is assigned using a multivariate regression. The corrections are tuned on photon candidates mostly of lower energies than those entering the analysis. For this reason the energy scale of photons above $\approx 200\,GeV$ deviates slightly from unity. The residual shift, due to the energy dependence of the longitudinal non-containment of the photon shower, is below 0.5% up to energies of $\approx 500\,GeV$ and below 1% up to energies of $\approx 1.5\,TeV$.

Discrepancies in the photon energy scale and resolution between data and simulation are resolved using dielectron events. Energy scale and resolution corrections are derived primarily from $Z \to e^+e^-$ events, using the procedure described in Ref. [29]. The corrections are derived in eight bins defined in terms of the R_9 variable (defined as the ratio between the energy deposited in the central 3x3 crystal matrix and the full cluster energy) and of $|\eta_{SC}|$.

The size of the energy scale corrections derived from $Z \to e^+e^-$ events is of the order of $0.5(1.5)\%$ for photon candidates in the $B = 3.8\,T$ ($B = 0\,T$) dataset, while the additional Gaussian smearing needed to match the energy resolution in simulated events with that in data varies between roughly 0.8% and 1.5% for photon candidates in the ECAL barrel region and between 2% and 2.5% for photon candidates in the endcap regions. The size of the additional Gaussian smearing measured for the $B = 3.8\,T$ and $B = 0\,T$ datasets are compatible within uncertainties. The dielectron invariant mass distribution obtained, for data and simulated events, after the adjustment procedure is shown in Fig. 3. To obtain these distributions, events containing pairs of photon candidates which satisfy the identification criteria used in the analysis and which are associated with electron tracks are selected. From Fig. 3 it can be noticed that narrower distributions are reconstructed for the $B = 0\,T$ dataset, compared to the $B = 3.8\,T$ one. This is due to the fact that a better collection of the electrons energy is achieved in the detector in the absence of the magnetic field. The most probable value of both distributions deviates from the nominal value of the Z mass because the electron energies are estimated using energy regression corrections tuned for photon candidates.

The stability of the correction factors as a function of the energy of the photon candidate is assessed using $Z \to e^+e^-$ events in which the Z boson is produced at high transverse momentum. This allows to test the transverse energy range up to roughly 150(100) GeV in the barrel (endcap) region. For the barrel region in the both the $B = 3.8\,T$ and $B = 0\,T$ datasets, the energy scale corrections are found to be stable within 0.5% in the probed range. A stability better than 0.7% is observed for the photon candidates in the endcaps.

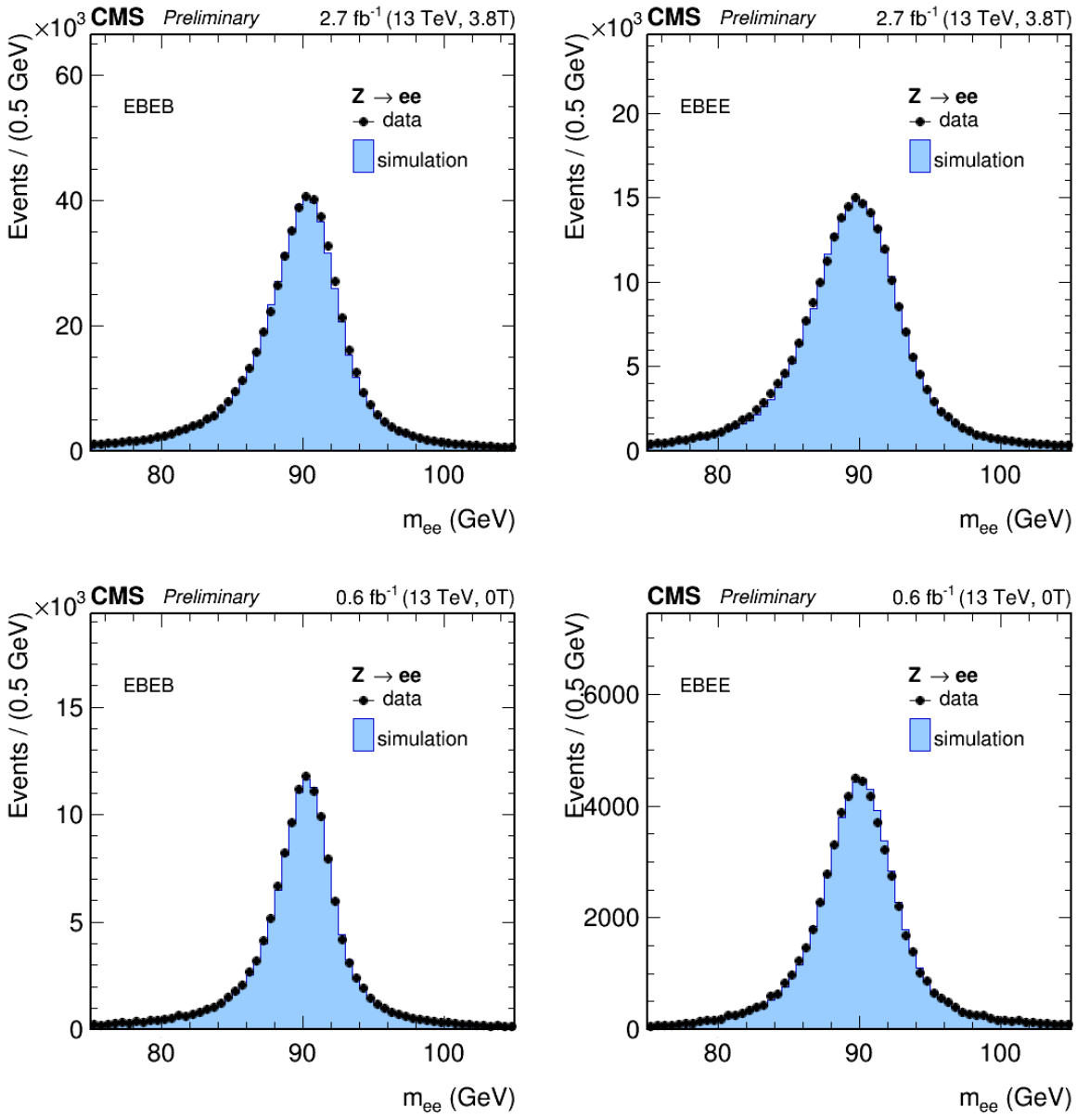

Figure 3: Comparison between the predicted and observed invariant mass distribution of electron pairs obtained after the application of energy scale and resolution corrections. Pairs of photon candidates satisfying the analysis identification criteria and compatible with electrons tracks are selected. Distributions are shown for events where both electrons are reconstructed in the barrel (left) and events where one electron is in an endcap (right). The top (bottom) row refers to the $B = 3.8\,T$ ($B = 0\,T$) datasets. The simulation predictions are scaled to match the number of events observed in data.

6 Diphoton mass spectrum

In the B = 3.8 T data sample, a total of 1236 (665) diphoton pairs are selected in the EBEB (EBEE) category. Out of these, 97 (184) pairs have an invariant mass above 500 GeV. In the B = 0 T data sample, a total of 278 (118) diphoton pairs are selected in the EBEB (EBEE) category. Out of these, 13 (37) pairs have an invariant mass above 500 GeV.

The invariant mass distribution of the selected events is shown in Fig. 4. A parametrisation of the spectrum of the form $f(m_{\gamma\gamma}) = m_{\gamma\gamma}^{a+b\cdot\log(m_{\gamma\gamma})}$, obtained through an unbinned maximum likelihood fit to the selected events, is shown. This parametric form corresponds to the one chosen to model the background in the hypothesis tests, as detailed in Section 9.

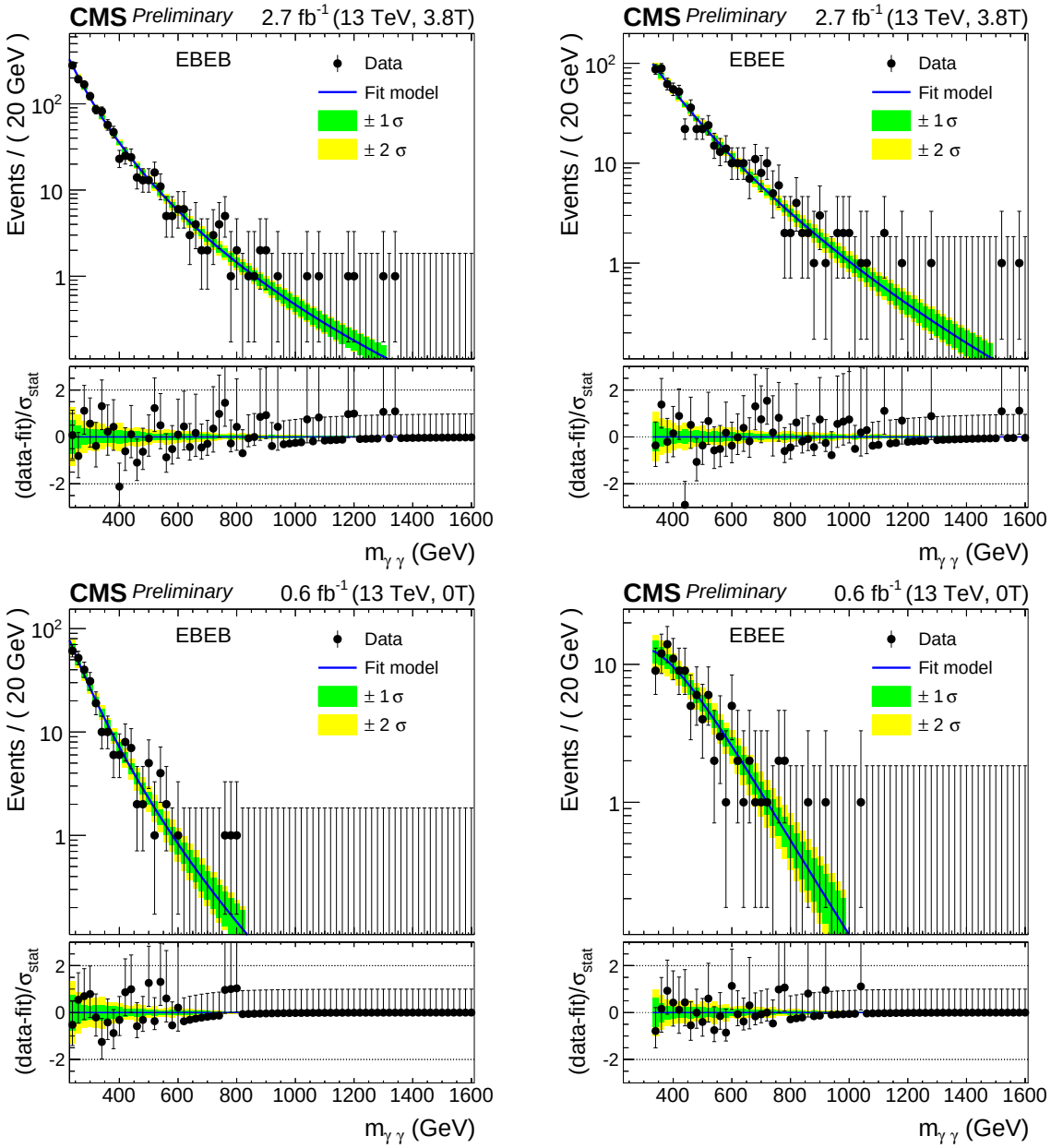

Figure 4: Observed invariant mass spectra for the EBEB (left) and EBEE (right). Top (bottom) row shows the B = 3.8 T (B = 0 T) dataset. The results of parametric fits to the data are also shown.

m (GeV)	$\sigma^{3.8T}_{FWHM}/m$		σ^{0T}_{FWHM}/m	
	EBEB	EBEE	EBEB	EBEE
500	0.94×10^{-2}	1.5×10^{-2}	1.05×10^{-2}	1.6×10^{-2}
1000	0.94×10^{-2}	1.5×10^{-2}	1.05×10^{-2}	1.5×10^{-2}
2000	0.96×10^{-2}	1.4×10^{-2}	1.05×10^{-2}	1.5×10^{-2}
4500	1.11×10^{-2}	1.4×10^{-2}	1.2×10^{-2}	1.4×10^{-2}

Table 1: Intrinsic mass resolution, evaluated as ratio between the full width at half maximum of the $m_{\gamma\gamma}$ distribution, for narrow-width signals, and the its probable value, further divided by 2.35 as a function of the resonance mass for the event categories used in the analysis.

7 Statistical analysis

The results of the search are interpreted in the frame of a composite statistical hypothesis test. A simultaneous fit to the invariant mass spectra of the EBEB and EBEE event categories is used to study the compatibility of the data with the background-only and the signal+background hypotheses.

The test statistics used in the hypothesis tests are based on the profile likelihood ratio:

$$q(\mu) = -2log\frac{L(\mu\cdot S + B|\hat{\underline{\theta}}_{\mu})}{L(\hat{\mu}\cdot S + B|\hat{\underline{\theta}})}$$

where S and B are the probability density functions for the resonant diphoton production process and the SM backgrounds respectively, μ is the so-called "signal strength" parameter and $\underline{\theta}$ are the nuisance parameters of the model, used to model systematic uncertainties. The $\hat{x}$ notation indicates the best-fit value of the parameter x, while the notation $\hat{x}_y$ denotes the best-fit value of x conditional on y.

8 Signal modelling

The signal distribution in $m_{\gamma\gamma}$ is determined from the convolution of the intrinsic shape of the resonance and the ECAL detector response. The intrinsic shape of the resonant signals are derived using the PYTHIA generator. A fine grid of mass points with 125 GeV spacing is used and the resulting shapes interpolated to intermediate points using the "moment morphing" technique described in [41]. The detector response is determined using fully simulated signal samples of small intrinsic width and corrected for the additional Gaussian smearing determined from dielectron events. Nine equidistant mass hypotheses in the range 500-4500 GeV are employed.

In order to determine the signal normalisation, the efficiency of the final event selection is combined with the kinematic acceptance. The first is obtained from fully simulated samples and interpolated using a quadratic function of the resonance mass. The second is obtained from the finely spaced grid of samples and parametrised as a quadratic function of both the resonance mass and width. A summary of the width of the signal reconstructed mass distribution, quantified through its full width at half maximum is reported in Table 1, while the functions accounting for selection efficiency and acceptance are shown in Fig. 2.

9 Background modelling

The background $m_{\gamma\gamma}$ spectrum is described by a parametric function of $m_{\gamma\gamma}$. The parametric coefficients are obtained from a fit to the data events, and considered as unconstrained nuisance parameters in the hypothesis test, allowing the building a data-driven description of the shape.

The accuracy of the background determination is assessed using MC simulations and it is quantified by studying the difference between the true and predicted number of background events in 14 $m_{\gamma\gamma}$ windows in the search region. Pseudo-experiments are drawn from the mass spectrum predicted by MC simulation. The total number of events in each pseudo-experiment is taken from a Poisson distribution where the mean is determined by the observation in data. For each mass window, the distribution of the pull variable, defined as the difference between the true and predicted number of events divided by the estimated statistical uncertainty, is constructed. If the absolute value of the median of this distribution is found to be above 0.5 in a window, an additional uncertainty is assigned to the background parametrisation. A modified pull distribution is then constructed increasing the statistical uncertainty on the fit by an extra term, denoted as the bias term, which is parametrised as a smooth function of $m_{\gamma\gamma}$, tuned in such a way that the absolute value of the median of the modified pull distribution is below 0.5 for all regions.

In order to account for this uncertainty in the hypothesis test, a signal-like term is added to the background model. The normalisation of such a term is taken to be normally distributed with a width determined by the integral of the bias term over the full-width at half-maximum of the tested signal shape. The uncertainties are evaluated independently for each of the four analysis categories and are assumed to be uncorrelated.

10 Systematic uncertainties

In this analysis the impact of the systematic uncertainties is smaller than that of the statistical uncertainties. The parametric background model has no associated systematic uncertainties, except for the bias term uncertainty described above. The shape coefficients are treated as unconstrained nuisance parameters, thus the associated uncertainties contribute to the statistical uncertainty.

Uncertainties associated to the signal modelling are summarised here:

- Luminosity uncertainty. For the $B = 3.8\,T$ dataset, a 2.7% [42] on the signal normalisation was assigned to reflect the uncertainty on the knowledge of the total integrated luminosity. For the $B = 0\,T$ dataset a 12% uncertainty was used instead. The two uncertainties were assumed to be uncorrelated.
- Selection efficiency uncertainties. For $B = 3.8\,T$, an 8% uncertainty on the signal normalisation was included to reflect the uncertainty on the knowledge of the selection efficiency. For the $B = 0\,T$ dataset a 16% uncertainty was used. Uncorrelated uncertainties were assumed for the two datasets.
- Parton distribution functions. A 6% uncertainty on the signal normalisation was assigned in order to account for the variation in the kinematic acceptance of the analysis coming from the use of alternative PDF sets.
- Photon energy scale uncertainty. For both the $B = 3.8\,T$ and $B = 0\,T$ dataset a 1% energy scale uncertainty was assign. This number was derived to take into account the knowledge of the energy scale at the Z peak and of its extrapolation to higher masses. Correlated uncertainties were assumed for the two datasets. In the case of

the 0T dataset, an additional 1% uncertainty was included to take into account the possible mismodelling of the difference in energy scale between the two datasets.

- Photon resolution uncertainty. The uncertainty on the resolution corrections factors is evaluated summing and subtracting 0.5% in quadrature from the estimated additional Gaussian smearing measured at the Z peak. Uncorrelated uncertainties were assumed for 0 and 3.8T.

11 Results of the search at 13 TeV

To set upper limits on the resonant diphoton production rate, the modified frequentist method, commonly known as CL_s is used following the prescription described in Ref. [43]. Asymptotic formulae [44] are used in the calculation. The validity of such formulae in the regime of this analysis was verified for a subset of the hypothesis tests. Expected and observed upper limits on the production of scalar and RS graviton resonances are shown in Fig. 5 for values Γ/m of 1.4×10^{-4}, 1.4×10^{-2} and 5.6×10^{-2}.

The compatibility of the observation with the background-only hypothesis is evaluated computing the background-only p-value. The latter is defined as the probability, in the background-only hypothesis, for $q(0)$ to be above the observation. This quantity, the "local p-value" p_0, does not take into account the fact that many signal hypotheses are tested. Asymptotic formulas are used to compute p_0 as a function of the resonance mass and width hypotheses. The validity of the formulas has been verified for a subset of the points.

The value of p_0 for different signal hypotheses is shown in Fig. 6. The largest excess observed in data has a p_0 value corresponding to 2.9 standard deviations. It is observed when testing for the production of an RS graviton with $m_G = 760\,\text{GeV}$ and $\Gamma/m = 1.4 \times 10^{-2}$. For the same mass and width, the scalar signal hypothesis has a p_0 corresponding to 2.85 standard deviations. Figure 7 shows, for $\Gamma/m = 1.4 \times 10^{-2}$, the contributions of the $B = 3.8\,\text{T}$ and $B = 0\,\text{T}$ dataset to the observed result in the mass range up to 850 GeV. The probability of observing an excess more significant than this for at least one of the signal spin and width hypotheses in the mass range between 500 GeV and 4.5 TeV is estimated constructing the sampling distribution of $\max(p_0)$ on an ensemble of background-only pseudo-experiments. The significance of the excess is estimated to be less than one standard deviation after taking this into account.

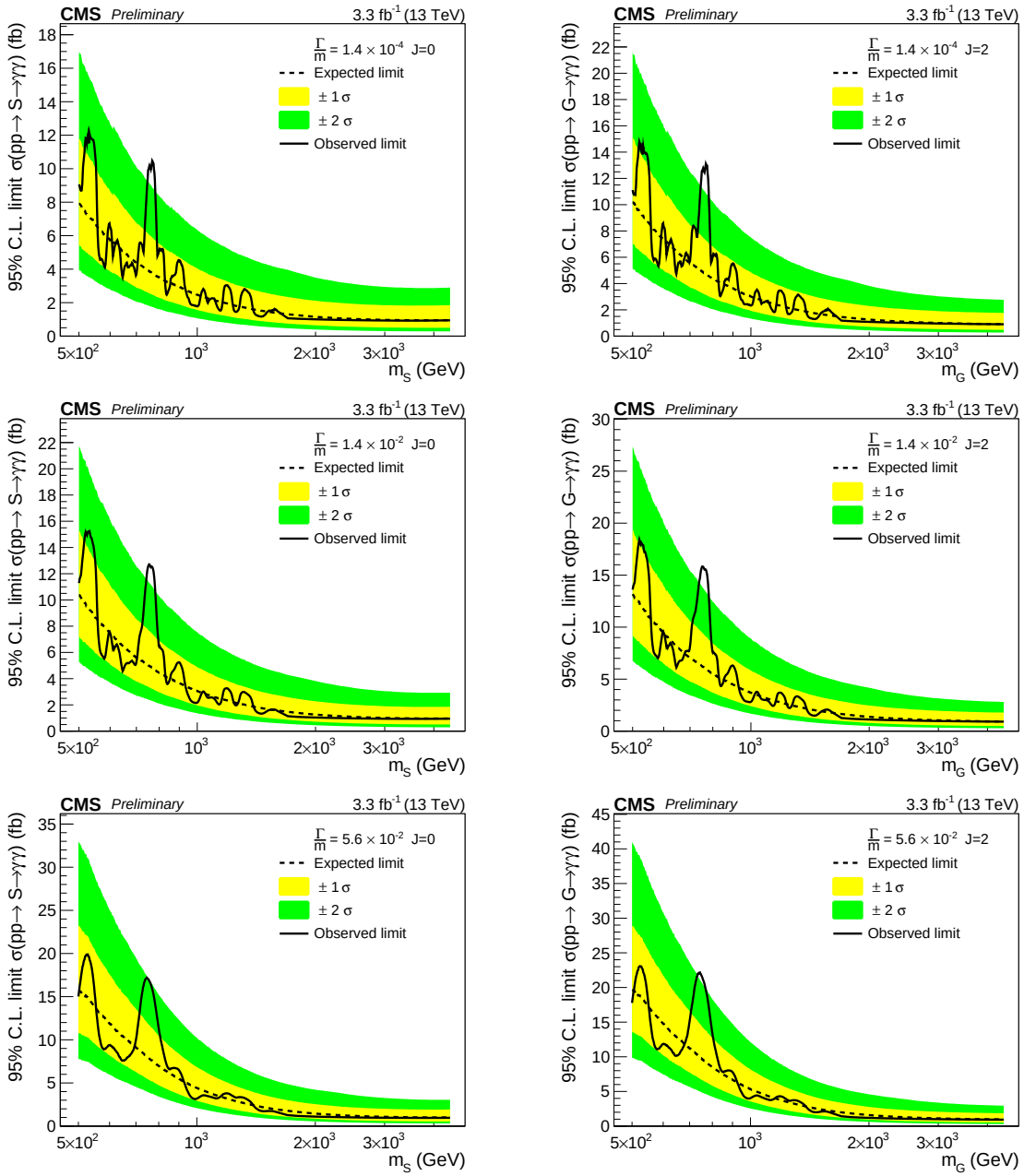

Figure 5: Expected and observed 95% C.L. exclusion limits for different signal hypotheses. The range 500 GeV $< m <$ 4.5 TeV is shown for $\Gamma/m = 1.4 \times 10^{-4}, 1.4 \times 10^{-2}, 5.6 \times 10^{-2}$. The left (right) column corresponds to the scalar (RS graviton) signals.

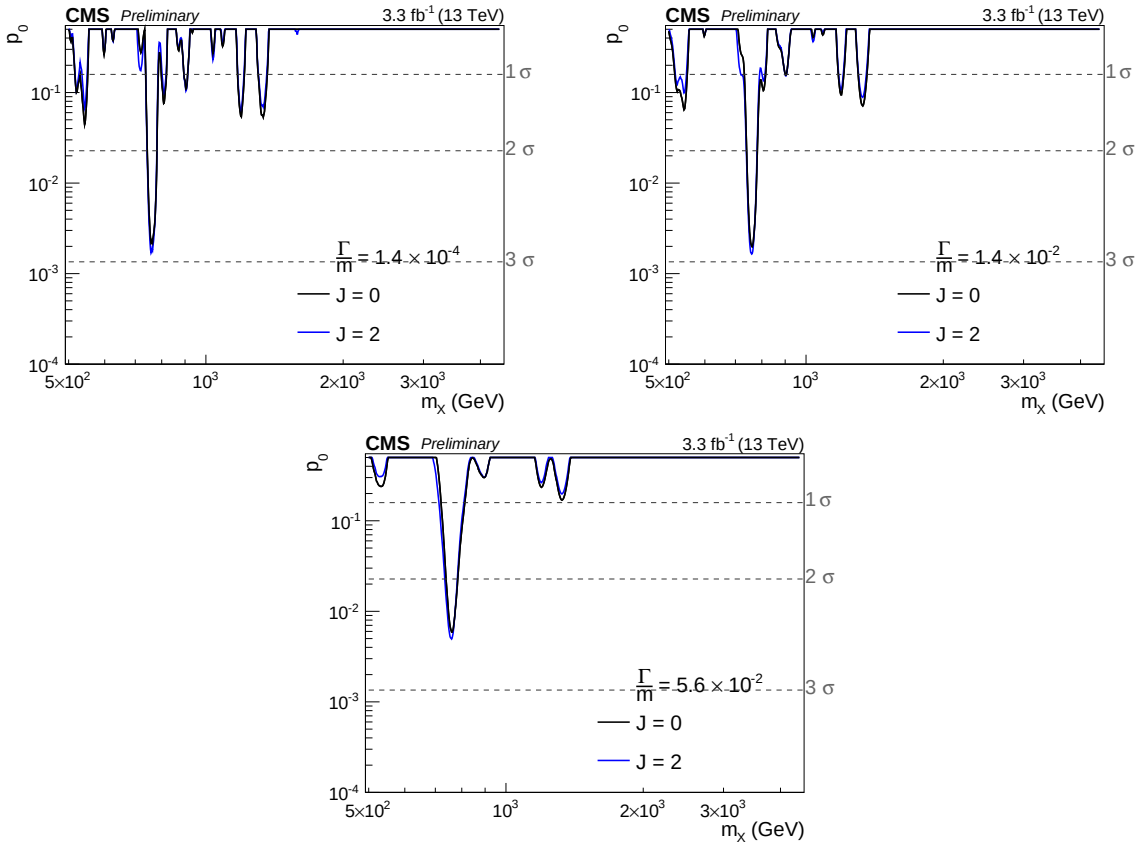

Figure 6: Observed background-only p-value for different signal hypotheses. The range $500\,\text{GeV} < m < 4.5\,\text{TeV}$ is shown for $\Gamma/m = 1.4 \times 10^{-4}, 1.4 \times 10^{-2}, 5.6 \times 10^{-2}$. Results corresponding to both the scalar and RS graviton hypotheses are shown.

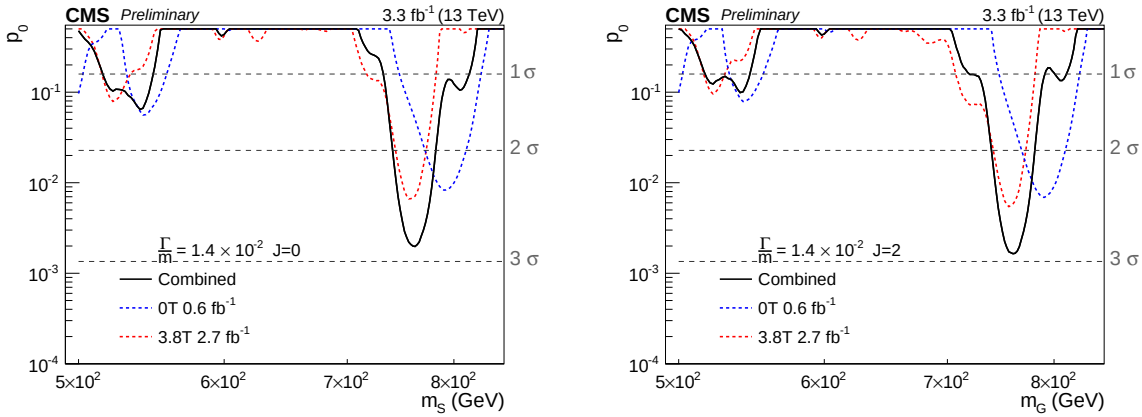

Figure 7: Observed background only p-values obtained on the 13 TeV dataset. The mass range $500\,\text{GeV} < m < 850\,\text{GeV}$ is shown is for resonances of $\Gamma/m = 1.4 \times 10^{-2}$. The contributions of the $\text{B} = 3.8\,\text{T}$ and $\text{B} = 0\,\text{T}$ datasets are shown separately. Due to the different size of the two datasets, the weight of the $\text{B} = 0\,\text{T}$ categories in the combined result is, at m = 760 GeV, roughly one fifth of that of the $\text{B} = 3.8\,\text{T}$ ones. The left (right) plot corresponds to the scalar (RS graviton) hypotheses.

12 Combined analysis of $\sqrt{s}$ = 8 TeV and 13 TeV datasets

The results obtained on the 13 TeV dataset are combined statistically with those obtained on the data recorded by the CMS experiment at the centre of mass energy of 8 TeV. Two analyses were performed by the CMS collaboration to search for diphoton resonances using the 8 TeV dataset. The analysis described in Ref. [16] searched for diphoton resonances in the mass range between 150 and 850 GeV, interpreting the results both in terms of production of scalar particles and in terms of production of RS gravitons. The analysis described in Ref. [17] focused on the mass range above 500 GeV and on the RS graviton hypothesis.

The statistical combination of the results is performed for all signal hypotheses which are tested for the 13 TeV analysis. The ratio of the signal production cross sections at $\sqrt{s}$ = 8 TeV and 13 TeV has been calculated using PYTHIA. It is roughly 0.29(0.27) for m_G (m_S) = 500 GeV and decreases to 0.04(0.03) when m_G (m_S) = 3 TeV. For m_G (m_S) = 750 GeV we find a cross section ratio of 0.24(0.22). No uncertainty is assigned to these values in the combined analysis.

The statistical treatment of the data analysed in Ref. [17] has been revisited. Exclusion limits are computed using the modified frequentest approach (as opposed to the Bayesian approach used originally). For this, the background is modelled using a parametric function of $m_{\gamma\gamma}$, following the same approach developed for the analysis of the 13 TeV data. The upper exclusion limits on $\sigma_G \cdot \mathcal{B}_{\gamma\gamma}$ obtained with this modelling agree within roughly 5% with the one in Ref. [17]. No change to the statistical modelling of the data analysed in Ref. [16] has been performed.

The three analyses considered slightly differ in respect to the acceptance and the event categorisation. In particular, the analysis in Ref. [17] is restricted to photon candidates in the ECAL barrel, while that in Ref. [16] accepts events where one or more candidates are in the ECAL endcaps and in Ref. [16] the events are categorised both according to $|\eta_{SC}|$ and R_9 of the photon candidates.

Since the event samples selected by the two 8 TeV analyses partially overlap, only one of the two is considered for each hypothesis test. In particular, at each m, the analysis leading to the most stringent median expected exclusion limit on resonant diphoton production is taken. Following this criterion, we use the results of Ref. [16] for $m < 850$ GeV and those of Ref. [17] for $m > 850$ GeV.

The experimental systematic uncertainties on the signal normalisation are assumed to be uncorrelated between the 8 TeV and 13 TeV datasets, since they are mostly due to the finite statistical power of the respective control samples.

In Ref. [16] the uncertainties assigned to the energy scale of the photon candidates in the ECAL barrel and endcaps are 0.5% and 2% respectively. The same uncertainties are assumed here for the analysis of the data from Ref. [17]. A linear correlation of 0.5 is assumed for energy scale uncertainties of the photon candidates in the 8 TeV and 13 TeV datasets. Taking the linear correlation to be 0 or 1 changes the observed limits and significance by less than 5% with respect to taking 0.5.

In the combined analysis, a simultaneous fit to the $m_{\gamma\gamma}$ spectra in all the event categories is performed, assuming a common signal strength modifier for all categories. Upper limits are set using the CL_s method and background-only p-values are computed. Asymptotic formulae [44] are used in all calculations.

The expected and observed median 95% C.L. exclusion limits on the equivalent 13 TeV production cross section, $\sigma^{13\,\text{TeV}}_{G,S} \cdot \mathcal{B}_{\gamma\gamma}$, for the combined analysis are shown in Figure 8. For the signal hypotheses below roughly 1.5 TeV, the exclusion limits obtained with the combined analysis

are more stringent than those obtained individually on the 8 or 13 TeV datasets by 20-40%. In the region above 1.5 TeV the exclusion limit is determined mostly by the 13 TeV analysis.

The background only p-value, p_0, for the combined analysis is shown in Figure 9, for all the tested signal hypotheses. The largest excess is observed for the narrow width hypothesis at m_S = 750 GeV and has a local significance of approximately 3.4 standard deviations.

Since the 8 TeV analysis used partially overlapping data regions to search for different signal hypotheses, the $max(p_0)$ sampling distribution can not be easily computed from ensembles of pseudo-experiments. The trial factors associated with the simultaneous test of several signal hypotheses are estimated combining the asymptotic formulas described in Ref. [45] with the results of the pseudo-experiments obtained in the analysis of the 13 TeV data. The trial factors associated with the test of several mass hypotheses are estimated counting the number of times the observed cross the 0.5 standard deviations level and applying the asymptotic formulas from Ref. [45]. To account for the different widths and spin hypotheses tested, a correction factor is estimated using the results of the toy-experiments obtained in the analysis of 13 TeV data. As a result, the significance of the excess, taking into account the effect of testing all the signal hypotheses considered, is estimated to be approximately 1.6 standard deviations.

To further qualify the compatibility of the results obtained with 8 TeV and 13 TeV datasets, we compute the likelihoods of the fits to a signal plus background hypothesis as a function of the equivalent cross section (extrapolated to $\sqrt{s}$ = 13 TeV). Narrow scalar and RS graviton hypotheses with mass m = 750 GeV were chosen. The fits are performed separately for each of two datasets and for the combined analysis. The results are shown in Fig. 10, where it can be seen that the equivalent cross sections estimated for the two datasets are compatible with each other, under both spin hypotheses.

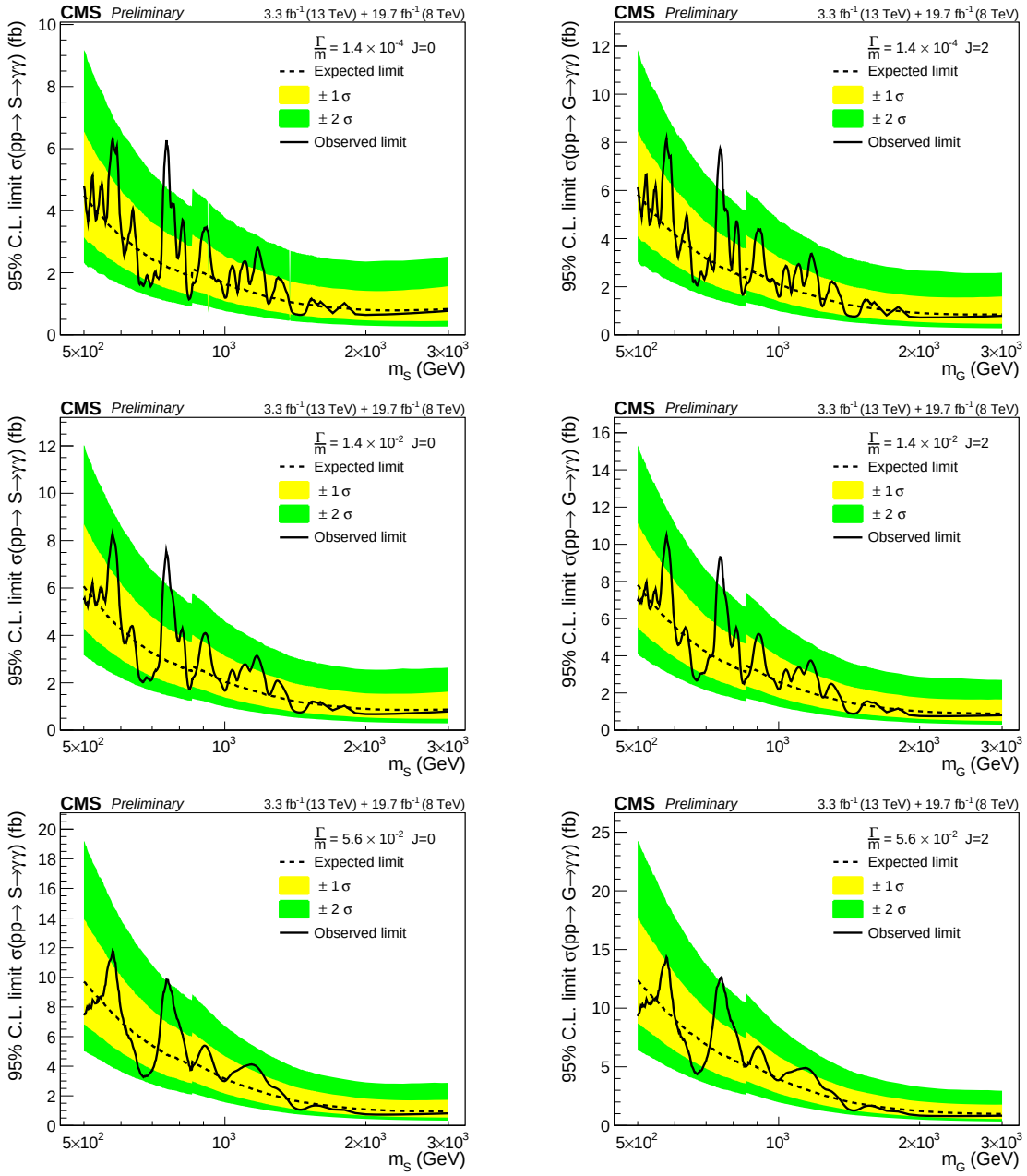

Figure 8: Upper limits on the production of high mass diphoton resonances obtained with the combined analysis of the 8 and 13 TeV data. The left (right) column corresponds to the scalar (RS graviton) signals. For $m < 850$ GeV, the results obtained at $\sqrt{s} = 8$ TeV with the analysis described in Ref. [16] are combined with those obtained at $\sqrt{s} = 13$ TeV. For $m > 850$ GeV the results of the analysis described in Ref. [17] obtained at 8 TeV are combined with those obtained at $\sqrt{s} = 13$ TeV.

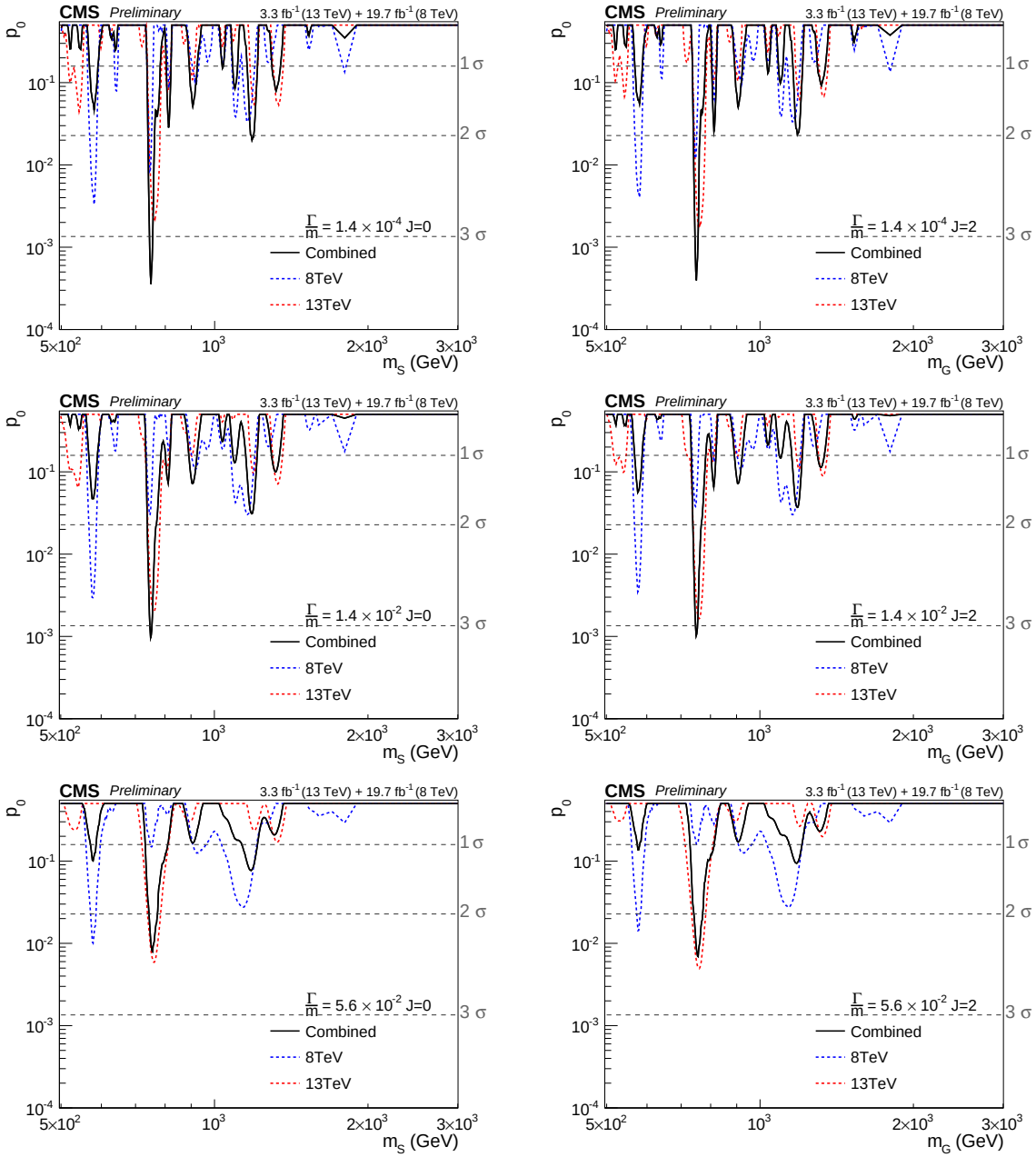

Figure 9: Observed background only p-values obtained from the combination of 8 TeV and 13 TeV results for different signal hypotheses. The contributions of the 8 and 13 TeV datasets are shown separately. At m = 750 GeV, the two datasets contribute with similar weights to the combined result. The left (right) column corresponds to the scalar (RS graviton) signals.

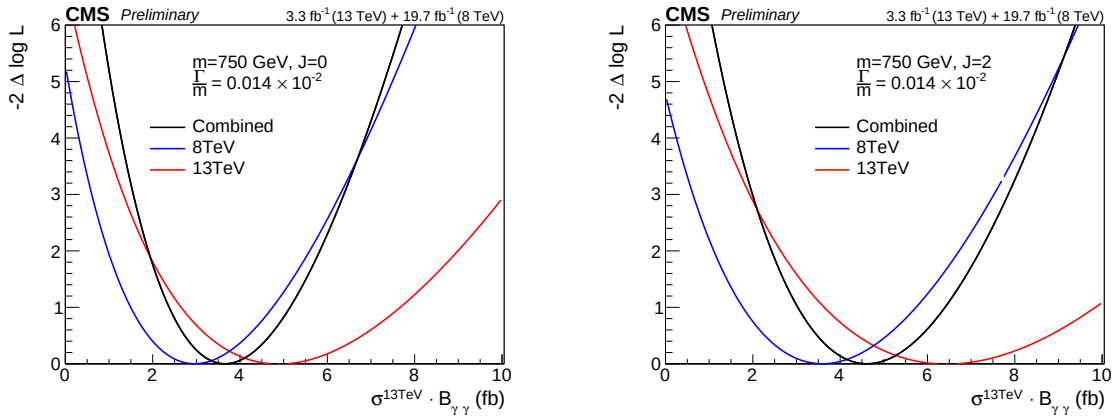

Figure 10: Likelihood scan for the cross section corresponding to the largest excess in the combined analysis of the 8 and 13 TeV datasets. The left (right) column corresponds to the scalar (RS graviton) signals. The 8 TeV results are scaled by the expected ratio of cross sections in each scenarios.

13 Summary

A search for new physics using the diphoton mass spectrum has been presented. The analysis is based on 3.3 fb^{-1} of pp collisions collected by the CMS experiment in 2015 at $\sqrt{s}$ = 13 TeV. Events containing two photon candidates with transverse momenta above 75 GeV were selected. The mass spectrum above 500 GeV was inspected to search for the production of spin-0 and spin-2 resonances.

The results of the search extend and supersede those previously reported by the CMS collaboration in Ref. [15]. The use of a new detector calibration and the inclusion in the analysis of additional data, recorded while the CMS magnet was not operated, improved the sensitivity of the analysis by more than 20% with respect to the previous results.

Limits on the production of scalar resonances and Randall-Sundrum gravitons in the range where 500 GeV $< m <$ 4.5 TeV and $\Gamma/m < 5.6 \times 10^{-2}$ were set using the modified frequentist approach. The largest excess is observed for $m = 760$ GeV and $\Gamma/m = 1.4 \times 10^{-2}$ and has a local significance of 2.8-2.9 standard deviations depending on the spin hypothesis. After taking into account the effect of searching for several signal hypotheses, the significance of the excess is reduced to less than one standard deviation. These observations are in agreement with what was reported in Ref. [15].

The results of the search are combined statistically with those obtained in similar searches at $\sqrt{s}$ = 8 TeV in the mass range 500 GeV $< m <$ 3.5 TeV and $\Gamma/m < 5.6 \times 10^{-2}$. The combined analysis improves the sensitivity of the individual analyses by 20-40% in the mass range up to roughly 2.5 TeV. The largest excess is observed in the combined analysis for $m = 750$ GeV and $\Gamma/m = 1.4 \times 10^{-4}$. The local p-value corresponds to approximately 3.4 standard deviations, which are reduced to approximately 1.6 standard deviations after taking into account the effect of searching for several signal hypotheses.

The reported results set stringent constraints on the production of scalar and RS graviton diphoton resonance in the mass range above 500 GeV.

References

[1] L. D. Landau, "The moment of a 2-photon system", *Dokl. Akad. Nauk SSSR* **60** (1948) 207.

[2] C. N. Yang, "Selection Rules for the Dematerialization of a Particle into Two Photons", *Phys. Rev.* **77** (1950) 242, doi:10.1103/PhysRev.77.242.

[3] N. Arkani-Hamed, S. Dimopoulos, and G. Dvali, "The Hierarchy problem and new dimensions at a millimeter", *Phys.Lett.* **B429** (1998) 263–272, doi:10.1016/S0370-2693(98)00466-3, arXiv:hep-ph/9803315.

[4] L. Randall and R. Sundrum, "A Large mass hierarchy from a small extra dimension", *Phys. Rev. Lett.* **83** (1999) 3370–3373, doi:10.1103/PhysRevLett.83.3370, arXiv:hep-ph/9905221.

[5] G. F. Giudice, R. Rattazzi, and J. D. Wells, "Quantum gravity and extra dimensions at high-energy colliders", *Nucl. Phys.* **B544** (1999) 3–38, doi:10.1016/S0550-3213(99)00044-9, arXiv:hep-ph/9811291.

[6] E. A. Mirabelli, M. Perelstein, and M. E. Peskin, "Collider signatures of new large space dimensions", *Phys. Rev. Lett.* **82** (1999) 2236–2239, doi:10.1103/PhysRevLett.82.2236, arXiv:hep-ph/9811337.

[7] T. Han, J. D. Lykken, and R.-J. Zhang, "On Kaluza-Klein states from large extra dimensions", *Phys. Rev.* **D59** (1999) 105006, doi:10.1103/PhysRevD.59.105006, arXiv:hep-ph/9811350.

[8] J. L. Hewett, "Indirect collider signals for extra dimensions", *Phys. Rev. Lett.* **82** (1999) 4765–4768, doi:10.1103/PhysRevLett.82.4765, arXiv:hep-ph/9811356.

[9] H. Davoudiasl, J. L. Hewett, and T. G. Rizzo, "Phenomenology of the Randall-Sundrum Gauge Hierarchy Model", *Phys. Rev. Lett.* **84** (2000) 2080, doi:10.1103/PhysRevLett.84.2080, arXiv:hep-ph/9909255.

[10] N. Craig, J. Galloway, and S. Thomas, "Searching for signs of the second Higgs doublet", (2013). arXiv:1305.2424.

[11] ATLAS Collaboration, "Observation of a new particle in the search for the Standard Model Higgs boson with the ATLAS detector at the LHC", *Phys. Lett.* **B716** (2012) 1–29, doi:10.1016/j.physletb.2012.08.020, arXiv:1207.7214.

[12] CMS Collaboration, "Observation of a new boson at a mass of 125 GeV with the CMS experiment at the LHC", *Phys. Lett.* **B716** (2012) 30–61, doi:10.1016/j.physletb.2012.08.021, arXiv:1207.7235.

[13] P. S. B. Dev and A. Pilaftsis, "Maximally symmetric two Higgs doublet model with natural standard model alignment", (2014). arXiv:1408.3405.

[14] ATLAS Collaboration, "Search for resonances decaying to photon pairs in 3.2 fb^{-1} of pp collisions at $\sqrt{s}$ = 13 TeV with the ATLAS detector", Technical Report ATLAS-CONF-2015-081, Dec, 2015.

[15] CMS Collaboration, "Search for new physics in high mass diphoton events in proton-proton collisions at $\sqrt{s} = 13$ TeV", CMS Physics Analysis Summary CMS-PAS-EXO-15-004, 2015.

[16] CMS Collaboration, "Search for diphoton resonances in the mass range from 150 to 850 GeV in pp collisions at $\sqrt{s} = 8$ TeV", *Phys. Lett.* **B750** (2015) 494–519, doi:10.1016/j.physletb.2015.09.062, arXiv:1506.02301.

[17] CMS Collaboration, "Search for High-Mass Diphoton Resonances in pp Collisions at $\sqrt{s} = 8$ TeV with the CMS Detector", CMS Physics Analysis Summary CMS-PAS-EXO-12-045, CERN, 2015.

[18] ATLAS Collaboration, "Search for high-mass diphoton resonances in pp collisions at $\sqrt{s} = 8$ TeV with the ATLAS detector", *Phys. Rev.* **D92** (2015), no. 3, 032004, doi:10.1103/PhysRevD.92.032004, arXiv:1504.05511.

[19] ATLAS Collaboration, "Search for Extra Dimensions in diphoton events using proton-proton collisions recorded at $\sqrt{s} = 7$ TeV with the ATLAS detector at the LHC", *New J. Phys.* **15** (2013) 043007, doi:10.1088/1367-2630/15/4/043007, arXiv:1210.8389.

[20] CMS Collaboration, "Search for signatures of extra dimensions in the diphoton mass spectrum at the Large Hadron Collider", *Phys. Rev. Lett.* **108** (2012) 111801, doi:10.1103/PhysRevLett.108.111801, arXiv:1112.0688.

[21] ATLAS Collaboration, "Search for high-mass dilepton resonances in pp collisions at $\sqrt{s} = 8$ TeV with the ATLAS detector", *Phys. Rev.* **D90** (2014), no. 5, 052005, doi:10.1103/PhysRevD.90.052005, arXiv:1405.4123.

[22] CMS Collaboration, "Search for heavy narrow dilepton resonances in pp collisions at $\sqrt{s} = 7$ TeV and $\sqrt{s} = 8$ TeV", *Phys. Lett.* **B720** (2013) 63–82, doi:10.1016/j.physletb.2013.02.003, arXiv:1212.6175.

[23] CMS Collaboration, "Search for narrow resonances using the dijet mass spectrum in pp collisions at $\sqrt{s}$=8 TeV", *Phys. Rev.* **D87** (2013), no. 11, 114015, doi:10.1103/PhysRevD.87.114015, arXiv:1302.4794.

[24] ATLAS Collaboration, "Search for new phenomena in the WW to $\ell\nu\ell'\nu'$ final state in pp collisions at $\sqrt{s} = 7$ TeV with the ATLAS detector", *Phys. Lett.* **B718** (2013) 860–878, doi:10.1016/j.physletb.2012.11.040, arXiv:1208.2880.

[25] CDF Collaboration, "Search for New Dielectron Resonances and Randall-Sundrum Gravitons at the Collider Detector at Fermilab", *Phys. Rev. Lett.* **107** (2011) 051801, doi:10.1103/PhysRevLett.107.051801, arXiv:1103.4650.

[26] D0 Collaboration, "Search for Randall-Sundrum Gravitons in the Dielectron and Diphoton Final States with 5.4 fb^{-1} of data from $p\bar{p}$ Collisions at $\sqrt{s} = 1.96$ TeV", *Phys. Rev. Lett.* **104** (2010) 241802, doi:10.1103/PhysRevLett.104.241802, arXiv:1004.1826.

[27] ATLAS Collaboration, "Search for Scalar Diphoton Resonances in the Mass Range 65–600 GeV with the ATLAS Detector in pp Collision Data at $\sqrt{s} = 8$ TeV", *Phys. Rev. Lett.* **113** (2014) 171801, doi:10.1103/PhysRevLett.113.171801.

[28] CMS Collaboration, "The CMS experiment at the CERN LHC", *JINST* **3** (2008) S08004, doi:10.1088/1748-0221/3/08/S08004.

[29] CMS Collaboration, "Performance of photon reconstruction and identification with the CMS detector in proton-proton collisions at $\sqrt{s} = 8$ TeV", *JINST* **10** (2015) P08010, doi:10.1088/1748-0221/10/08/P08010, arXiv:1502.02702.

[30] CMS Collaboration, "Particle-flow event reconstruction in CMS and performance for jets, taus, and $E_{\mathrm{T}}^{\mathrm{miss}}$", CMS Physics Analysis Summary CMS-PAS-PFT-09-001, 2009.

[31] CMS Collaboration, "Commissioning of the particle-flow event with the first LHC collisions recorded in the CMS detector", CMS Physics Analysis Summary CMS-PAS-PFT-10-001, 2010.

[32] T. Sjöstrand et al., "An Introduction to PYTHIA 8.2", *Comput. Phys. Commun.* **191** (2015) 159–177, doi:10.1016/j.cpc.2015.01.024, arXiv:1410.3012.

[33] R. D. Ball et al., "Parton distributions with LHC data", *Nucl. Phys.* **B867** (2013) 244–289, doi:10.1016/j.nuclphysb.2012.10.003, arXiv:1207.1303.

[34] T. Gleisberg et al., "Event generation with SHERPA 1.1", *JHEP* **02** (2009) 007, doi:10.1088/1126-6708/2009/02/007, arXiv:0811.4622.

[35] J. Alwall et al., "The automated computation of tree-level and next-to-leading order differential cross sections, and their matching to parton shower simulations", *JHEP* **07** (2014) 079, doi:10.1007/JHEP07(2014)079, arXiv:1405.0301.

[36] NNPDF Collaboration, "Parton distributions for the LHC Run II", *JHEP* **04** (2015) 040, doi:10.1007/JHEP04(2015)040, arXiv:1410.8849.

[37] CMS Collaboration, "Event generator tunes obtained from underlying event and multiparton scattering measurements", arXiv:1512.00815.

[38] GEANT4 Collaboration, "GEANT4 - a simulation toolkit", *Nucl. Instrum. Meth. A* **506** (2003) 250, doi:10.1016/S0168-9002(03)01368-8.

[39] CMS Collaboration, "Observation of the diphoton decay of the Higgs boson and measurement of its properties", *Eur. Phys. J.* **C74** (2014), no. 10, 3076, doi:10.1140/epjc/s10052-014-3076-z, arXiv:1407.0558.

[40] CMS Collaboration, "First results on Higgs to $\gamma\gamma$ at 13 TeV", CMS Physics Analysis Summary CMS-PAS-HIG-15-005, 2016.

[41] M. Baak, S. Gadatsch, R. Harrington, and W. Verkerke, "Interpolation between multi-dimensional histograms using a new non-linear moment morphing method", *Nucl. Instrum. Meth. A* **771** (2015) 39, doi:10.1016/j.nima.2014.10.033, arXiv:1410.7388.

[42] CMS Collaboration Collaboration, "CMS Luminosity Measurement for the 2015 Data Taking Period", Technical Report CMS-PAS-LUM-15-001, CERN, 2016.

[43] ATLAS and CMS Collaborations, LHC Higgs Combination Group, "Procedure for the LHC Higgs boson search combination in Summer 2011", ATL-PHYS-PUB/CMS NOTE 2011-11, 2011/005, 2011.

[44] G. Cowan, K. Cranmer, E. Gross, and O. Vitells, "Asymptotic formulae for likelihood-based tests of new physics", *Eur.Phys.J.* **C71** (2011) 1554, doi:10.1140/epjc/s10052-011-1554-0, 10.1140/epjc/s10052-013-2501-z, arXiv:1007.1727.

[45] E. Gross and O. Vitells, "Trial factors or the look elsewhere effect in high energy physics", *Eur. Phys. J.* **C70** (2010) 525–530, doi:10.1140/epjc/s10052-010-1470-8, arXiv:1005.1891.